Published in final edited form as:

CIRP J Manuf Sci Technol. 2021 January ; 32: . doi:10.1016/j.cirpj.2020.11.014.

On the interplay of friction and stress relaxation to improve stretch-flangeability of dual phase (DP600) steel

Kali Prasad[a], **Venkatesh B**[c], **Hariharan Krishnaswamy**[a,*], **Dilip K Banerjee**[b], **Uday Chakkingal**[c]

[a]Manufacturing Engineering Section, Department of Mechanical Engineering, IIT Madras, Chennai-600036, India

[b]Material Measurement Laboratory, National Institute of Standards and Technology(NIST), Gaithersburg, Maryland 20899, USA

[c]Metal Forming Laboratory, Department of Metallurgical and Materials Engineering, IIT Madras, Chennai-600036, India

Abstract

Industrial servo presses have been used to successfully demonstrate improved formability when deforming sheet metals. While the time dependent viscoplastic behavior of material is attributed to the observed formability improvement, much less effort has been devoted to understand and quantify the underlying mechanisms. In this context, the hole expansion test (HET) of a dual phase steel was interrupted at pre-defined punch travel heights to understand the time-dependent effects on stretch-flangeability. The effect of pre-strain, hold time and edge quality on hole expansion ratio (HER) improvement was studied. The present study shows that the HER improves significantly in interrupted HET. This improved HER is due to the combined effects of stress relaxation and friction on deformation behavior. The ductility improvement estimated from uniaxial stress relaxation tests was used to estimate the contribution of stress relaxation and friction, respectively, in HET. This study shows that friction plays a significant role in improving HER at high pre-strain. It was also demonstrated that frictional effects are largely influenced by edge quality.

Keywords

Stretch-flangeability; Hole expansion ratio; Dual phase steel Stress relaxation; Servo press; Finite element analysis

1. Introduction

Dual phase (DP) steels belong to the family of first generation advanced high strength steels (AHSS), which have a microstructure exhibiting two distinct phases, namely ferrite and martensite [1, 2]. DP steels, known for their excellent combination of strength and ductility,

*Corresponding author hariharan@iitm.ac.in (Hariharan Krishnaswamy).

exhibit poor stretch-flangeability [3, 4]. Stretch flangeability refers to the ability of the material to resist edge cracking during sheet metal forming operations [5]. In a typical sequence of multistage forming of sheet components, flanging is performed toward the later stages after large plastic strain and significant work hardening take place[6, 7]. Stretch-flangeability can be evaluated with the HET, where a circular blank with a central hole is deformed using a rigid punch. The central hole expands and the test is continued until the failure of sheet is indicated by the appearance of surface cracks. The ratio of the change in the initial hole diameter to the initial hole diameter estimated from HET is referred as the HER and is used to quantify the stretch-flangeability of the material [8]. Higher values of HER indicate better stretch-flangeability. The central hole of a standard HET specimen is usually punched, although other methods such as drilling, shearing, wire cut electrical discharge machining (EDM), laser trimming and reaming [3, 9, 10] have been used in the past. The HER estimated is highly sensitive to the process used for hole preparation due to the edge condition [11–13]. For instance, micro-cracks that typically form at the end machining step can possibly serve as damage initiation sites [3, 14, 15] during HET. This is further confirmed by the correlation between fracture toughness and HET as reported in literature [13, 16, 17]. The good correlation of HER prediction with damage models for different materials (miscrostructure) further proves that the edge condition rather than base microstructure plays a dominant role in determining the final HER values. Hole expansion occurs in routine forming operations. A traditional forming limit diagram (FLD) is not suitable for predicting edge cracking during stretching operations as failure is sensitive to the edge condition [3, 18]. In general, sheets with finished holes perform better than those with sheared edges. HER estimate is strain path dependent, as evident from its variation with punch geometry. It was shown that the failure region is subjected to a uniaxial state of stress when a conical punch is used and a plane strain state when a flat bottom punch is used [3, 19]. The state of stress is complex and varies continuously with deformation when using a hemispherical punch [19].

In addition to the effects of edge condition and punch shape, HER is dependent on the metallurgical parameters such as non-metallic inclusions [20], grain size [21, 22] and microstructure [23]. The relative strength difference between the soft ferrite and hard martensite plays an important role on the edge formability of DP steels [23, 24]. Fang et al. [23] investigated the effect of tempering temperature on hole expansion behavior of C-Mn steel and found that the HER increased after tempering due to the reduction of strength difference between ferrite and martensite phases.

As discussed above, HER is influenced by edge quality and loading path, in addition to microstructure. Therefore, for a given material (microstructure) HER can be improved by modifying the deformation process parameters and edge preparation. Although many attempts have been made to relate HER with tensile properties such as ultimate tensile strength (UTS) and uniform elongation, HER was found to correlate well with fracture strain or fracture toughness [13, 15, 25]. The onset of fracture during sheet metal forming can be postponed using non-conventional forming processes such as the servo press [26, 27]. The stepped punch travel using a servo press is known to improve the formability of sheet metals [26, 28, 29]. Altan and coworkers [30] have demonstrated that HER can be improved using servo press technology. Although the exact mechanism for formability improvement using a

servo press is not yet established, it is believed that stress relaxation phenomena [31] play an important role, while effects of other factors related to friction cannot be ignored. Controlled uniaxial stress relaxation tests have shown ductility improvement [1] in many alloys [32–35]. As mentioned earlier, the formability improvement when using a servo press could result from multiple factors including stress relaxation, strain path change and transient contact conditions. It is challenging to separate the contribution of each of these factors in deciphering the formability improvement using servo press. Since a uniaxial stress state exists at the edge condition of HET when using conical punch, a uniaxial test is expected to provide valuable insights on the role of other factors without the complications arising from multi-axial stress states and strain path changes.

In the present work, systematic investigation of stretch-flangeability in DP600 steel was performed. The first objective of the study is to determine the effect of stress relaxation on the hole expansion behavior of DP600. Standard hole expansion tests were conducted in two different test modes: (i) monotonic and (ii) interrupted. The latter mode can be used to correlate with uniaxial stress relaxation tests. Finite element simulation of HET is carried out to estimate the average strain rate at the hole edge where uniaxial stress state exists. The estimated strain rate is used to conduct uniaxial stress relaxation experiments. Single step stress relaxation experiments were conducted to study the influence of pre-strain and relaxation time on ductility improvement. The uniaxial tensile deformation was correlated with HER results. The second objective of the investigation is to quantify the contribution of stress relaxation on hole expansion behavior of DP600 using analysis of uniaxial stress relaxation tests. A detailed microstructural analyses of the failed samples after HET was also conducted using a scanning electron microscope.

2. Materials and Methods

The material used in the present work is hot rolled, pickled and oiled (HRPO) DP600 sheet with thickness 2.6 mm, obtained from ArcelorMittal [2]. The chemical composition of as received DP600 steel was measured using Optical Emission Spectroscopy (OES) and is listed in Table 1.

2.1. Uniaxial mechanical testing

Monotonic and stress relaxation tests were conducted using a Zwick Roell Z100 100 kN universal tensile testing machine equipped with an optical non contact video extensometer. Tensile specimens were prepared as per the ASTM E8 standard [36]. Stress relaxation tests were conducted by stopping the machine without unloading the specimen at a pre-defined strain for a known relaxation time. The tensile test was resumed post relaxation in the initial strain rate until fracture. Details of monotonic and stress relaxation experiments are tabulated in Table 2. All the experiments were repeated three times.

[1]Ductility in this manuscript refers to uniform elongation, unless otherwise stated

[2]Certain commercial equipment, instruments, software or materials are identified to describe a procedure or concept adequately. Such identification is not intended to imply recommendation, endorsement or implication by NIST that the equipment, instruments, software or materials identified are necessarily the best available for the purpose.

2.2. Hole expansion test

HET were performed on 90 × 90 mm^2 square sheets with a centre hole of diameter 10 mm using a conical punch with a cone angle of 60°. Central hole was prepared using drilling and boring process. Both the hole preparation techniques involved two stages. In the case of drilled hole, a 5 mm diameter central hole was drilled followed by 10 mm diameter drilling at 630 rpm. In the case of bored hole, 9.5 mm central hole was drilled followed by boring at 500 rpm using a single point boring tool. The lip angle of the drill bits used was 59°. Both the above process were performed in a vertical drilling machine (HMT - TRM 3V). Standard laboratory deburring technique using abrasive papers were used to remove the visible burrs. The deburring was limited to treating visible burrs so as to maintain the surface roughness during further processing.

A blank holder force of 65 kN was applied to hold the blank and prevent draw-in of the sheet. A video camera with a light source was used to record the images of the edge as the hole expanded and was viewed on a computer monitor. Testing was stopped on the visual detection of a through-thickness crack. HET was conducted as per the ISO 16630 2009 standard (Figure.1). In the present study, experiments (Figure.2) were conducted in two different modes (i) monotonic mode (punch continuously deforms the blank) (ii) interrupted mode, where the punch was stopped intermittently during the test. The hole expansion ratio (HER) value was calculated using equation (1).

$$HER(\%) = \frac{d_f - d_o}{d_o} \times 100 \tag{1}$$

where, d_f and d_o represents the final and initial diameter of the central hole. d_o is calculated using the average value of four diameters measured at angles of 45°.

The ductility improvement due to stress relaxation is sensitive to pre-strain, strain rate and hold time [33, 34]. In practice, punch travel can be correlated with the pre-strain in the sample. Two different punch displacement positions, 50% and 70% of maximum punch travel were chosen arbitrarily to perform interrupted HET. It was recently shown that [35] at room temperature, relaxation time greater than 60 s does not enhance the ductility significantly. Therefore, the holding time was limited to 60 s. In a typical production set up, holding time should be as minimum as possible to maximize the throughput. Hence a lower range of 10 s was used to quantify the contribution of stress relaxation on hold time. The experimental conditions of monotonic and interrupted HET are given in Table 3. Each test condition was repeated thrice and the average values along with standard deviations are reported.

Equivalent failure strains in HET were estimated using analytical equations developed by Butcher et al.[37] by measuring the inner hole diameter (d_{inner}), outer hole diameter (d_{outer}) and sheet thickness around the circumference at failure (t_{edge}):

$$\epsilon_{eq} = \frac{2}{3}(\epsilon_c - \epsilon_t) \tag{2}$$

where, ϵ_c and ϵ_t are circumferential and thickness, strain given by

$$\epsilon_c = \ln\left(\frac{d_{outer} + d_{inner}}{2d_o}\right)$$

$$\epsilon_t = \ln\left(\frac{t_{edge}}{t_o}\right)$$

where, d_o and t_o are initial hole diameter and sheet thickness respectively.

2.3. Finite element simulation of HET tests

Finite element analysis was performed using commercially available ABAQUS\Explicit 6.14 software. The conical punch was modelled as an analytically rigid body. The 90 × 90mm^2 rectangular blank with a central hole of 10 mm diameter and thickness of 2.6 mm was modelled as a deformable material. The rectangular blank was meshed using three dimensional continuum elements (C3D8R) with progressively finer mesh near the hole region. The through-thickness direction of the blank was meshed with at least 10 elements considering the large local bending deformation. The contact between tool and blank was modelled assuming Coulomb friction with a coefficient of 0.2 [10]. The punch was constrained to move only in the vertical direction with a constant velocity of 10 mm/min. The edges of the blank were completely constrained for displacement and rotation. The mechanical behavior of the blank was assumed to follow the von Mises yield criterion, as the equivalent strain estimated for HET using equation (Eq.2) is valid only for isotropic materials. Finite element simulations performed did not show any measurable difference in the strain distribution (refer Appendix A) between von Mises and anisotropic Hill 48 yield criteria. Therefore, anisotropy of mechanical properties due to crystallographic texture was ignored in the present simulation. The strain hardening behavior of the material was modelled using the hybrid hardening law as in eq.3. The hybrid hardening law has been successfully used to describe the mechanical behavior including in the post necking region [38].

$$\sigma = \sigma_0 + zK\epsilon_p{}^n + (1-z)C\left(1 - e^{-\alpha\epsilon_p}\right) \quad (3)$$

Where, σ_0 is yield stress, ϵ_p is plastic strain, C, α, K, n are material constants and z is the weight factor ($0 \leq z \leq 1$) that is used to combine Swift and Voce hardening laws. The parameters of the combined Swift-Voce isotropic hardening law were obtained by least square fitting of the experimental true stress-true plastic strain data of uniform elongation from the uniaxial tensile tests. The weight factor, z, was estimated by fitting the post necking behavior of similar materials in literature [38]. Figure.3. shows the extrapolated true stress and true plastic strain data using this hybrid hardening law. The values of fitted parameters of the hardening model are tabulated in Table 4.

3. Results and discussion

The microstructure of the base metal is characterized. The characterization procedure and results can be referred to in Appendix B and C.

3.1. Ductility improvement: Uniaxial tensile test

The stress-strain response of the material subjected to monotonic and stress relaxation loading is shown in Figure.4. A strain rate of, $\dot{\epsilon} = 0.042\ s^{-1}$ was used to conduct monotonic and stress relaxation tests. This strain rate corresponds to the maximum value reached at hole edges during HET, as estimated from finite element analysis (Section 2.1). Improvement in ductility was observed when the tensile specimen was subjected to stress relaxation at different combinations of pre- strain and relaxation time. Following earlier literature [33–35], the improvement in ductility due to uniaxial stress relaxation is quantified using $\epsilon_r = \frac{\epsilon_{relax}}{\epsilon_{mono}}$, where ϵ_{relax} and ϵ_{mono} refers to true uniform elongations with and without stress relaxation, respectively.

Figure.5(a) and (b) shows the effects of pre-strain and relaxation time on ductility improvement, respectively. The ductility improvement (ϵ_r) increases with pre-strain and relaxation hold time, which are similar to the findings reported in the literature [33–35, 39]. The summary of ductility improvement due to stress relaxation are tabulated in Table 5

As reported in our earlier work [34, 35], the ϵ_r is empirically fit using regression analysis. $\varepsilon_r = f(\epsilon, \dot{\epsilon}, t)$; ($\epsilon, \dot{\epsilon}$ and t are true strain, true strain rate, and time, respectively). $\dot{\epsilon}$ and t are coupled to non-dimensionalize the variables of the regression equation. The empirical relation obtained for DP600 steel is expressed as (eq.4). The coefficient of determination, R^2, of the fit is 0.95.

$$\epsilon_r = 1.22 \times \left\{ \epsilon^{0.055} \times (\dot{\epsilon} \times t)^{0.0019} \right\} \tag{4}$$

3.2. Hole expansion test

HET were carried out as explained in Section 2.3. Holes were prepared both by drilling and boring. Material separation during machining processes such as drilling and boring induce micro-cracks on the surface that serve as crack initiation sites during HET. During the later stages of HET, through-thickness cracks developed and samples failed without localized necking. Microstructural investigation near the hole edge (Figure.6) reveals that crack propagated along the ferrite-martensite interface. Ferrite being a softer and more ductile phase compared to martensite, sustains large plastic deformation compared to martensite. This inhomogeneity in plastic deformation behavior of constituent phases initiates voids at the inter-phase boundaries [40–42] and possibly results in decohesion in the inter-phase region. Therefore, failure of the material at the hole edge plays a dominant role during HET.

Figure.7 shows HER (Eq.1) and equivalent failure strain (Eq.2) in drilled and bored edges. It is observed that bored edge samples failed at higher equivalent failure strain and thus

showed higher HER. This suggests that HER and equivalent failure strain value is sensitive to the initial hole preparation technique, in agreement with previously reported results [3, 9, 43, 44].

The observed difference in HER due to hole edge quality can be correlated with surface roughness (Figure.8). The measured average surface roughness (R_a) of a drilled hole edge is $4.32 \pm 0.192\ \mu m$ and that of a bored edge is $2.32 \pm 0.145\ \mu m$. The surface roughness of drilled edges is nearly twice that of the bored edge. As explained earlier, micro-cracks developed during the drilling process. The boring process is a finishing process, post drilling and hence the micro-cracks formed are relatively less than those at drilled edges. Since the machining parameters of both drilling and boring can influence the surface roughness, it is prudent to correlate the influence of hole edge using surface roughness rather than the manufacturing process. While such an attempt is of interest, the present work focuses on the time-dependent mechanical behavior on the HER improvement.

In addition to the edge surface, the stretch flangeability and therefore the HER can be improved by utilizing the mechanical viscoplastic behavior or rate effect of materials, as demonstrated in the application of a servo press [45]. Such time-dependent effects can be studied by interrupting the HET (refer to section.3.4) without unloading.

3.3. Finite element simulation of HET

One problem with the traditional evaluation of HER from a HET is the possibility of having non-uniform strains around the edges, which varies from that calculated with the analytical expression (equation 1) based on uniform change in diameter of the hole. Therefore, finite element modeling is routinely conducted to understand the overall deformation behavior and stress evolution during HET. Stress triaxiality values near the hole edge (shown in Figure.9. (a)) are in the range of (0.33 to 0.37), which is very close to the corresponding uniaxial stress state value (0.33). From the distribution of equivalent plastic strain and von Mises stress, Figure. 9.(b) and (c), it is concluded that deformation is primarily concentrated near the hole edge and a significant amount of stress concentration exists near the edge.

In order to evaluate the stress state of the hole edge, three elements (outer, middle and inner) were chosen along the through-thickness direction, as shown in Figure.10(a). The evolution of maximum and minimum principal strain with punch travel at outer, middle and inner edges is shown in Figure.10(b),(c) and (d), respectively. For isotropic materials, the strain path corresponding to the uniaxial state of stress is given by ($\epsilon_1 = -2\epsilon_2$). The estimated major and minor principal strains plotted in Figure.10(e) indicates that the outer and middle portions of the edge follow a uniaxial strain path. The inner edge, however deviates from the uniaxial strain path possibly due to varying compressive stresses and friction conditions between the sheet and the conical punch.

The experiments and FE results show that the HET is controlled by the hole edge state and the edge is predominantly under a uniaxial stress state. Thus, it is reasonable to relate the deformation behavior during a typical interrupted HET and uniaxial stress relaxation test. Any deviation between the trend of HET and uniaxial tension could therefore be attributed

to the friction effect during stress relaxation. The strain rate experienced by material at the hole edge is estimated not to exceed 0.042 s^{-1} as shown in Figure.11.

3.4. Interrupted HET

As schematically illustrated in Figure.2, interrupted HET was performed to simulate the effect of a servo press. Samples subjected to interrupted testing underwent larger failure strain compared to monotonic loading, thereby resulting in higher HER values. Figure.12 shows the sample before and after conducting HET in monotonic and interrupted modes.

As the punch motion was interrupted during HET, the material was subjected to stress relaxation which contributes to improved ductility [33–35, 39]. In addition to that, the elastic recovery during relaxation alters the contact stresses and possibly the contact area too. The above phenomenon, along with pressure dependent friction force at large plastic strain, influences the mechanical behavior of HET [46–48]. The net effect in HER is quantified using $\epsilon_\beta = \frac{\epsilon_{eq}^I}{\epsilon_{eq}^M}$ where, ϵ_{eq}^I and ϵ_{eq}^M refers to equivalent plastic strain (eq.2) at fracture in interrupted and monotonic loading, respectively. Under frictionless conditions, ϵ_{eq}^I is expected to follow the trend of uniaxial stress[3] relaxation. It is contended that the contact stresses due to friction alter the material behavior during relaxation. Therefore, it is pertinent to understand the interplay of material and friction effects. The material effect on ductility improvement due to stress relaxation has been reported earlier and is sensitive to relaxation time, pre-strain and strain rate [33, 34]. Accordingly, the failure strain in interrupted HET is expected to vary with hold time, punch depth and punch velocity. In an attempt to separate the friction effect, uniaxial stress relaxation tests were performed. The difference in the trend of ductility improvement in uniaxial tests (ϵ_r) and in HET (ϵ_β) could provide more insights on the role of friction in HER improvement during interrupted tests. In the present work, the punch velocity, which correlates with strain rate, was kept constant. The hold time and the punch depth (corresponding to pre-strain) were varied during HET, the results of which are shown in Figure.13 and tabulated in Table 6.In general, HER improvement is greater with longer hold time and higher punch depth, which is in agreement with the results seen during uniaxial stress relaxation tests. The trend of improvement is similar in both edge conditions (i.e., drilled and bored edges) during interrupted testing, however the bored edge showed larger improvement in HER.

One of the important advantages of choosing HET to study stress relaxation effects is the existence of a uniaxial stress state in the proximity of the hole edge where large deformation takes place. Unlike other tests such as deep drawing, HET avoids the complications in understanding the deformation behavior due to strain path effect and multi-axial stress state. Therefore, as mentioned earlier, in the special condition of a frictionless test, the HET improvement is expected to follow that obtained in uniaxial tensile test. Experimental verification of uniaxial stress state is difficult; numerical analysis performed in the present work is used to verify the stress state and the related mechanics of interrupted HET test.

[3]The stress state near the edges in HET is near uniaxial as subsequently discussed in section.3.3

3.5. Contribution of friction effect in HET

The overall HET improvement using interrupted loading is due to stress relaxation and friction effects. As indicated earlier, it is of interest to decouple these effects for efficient process design in use of a servo press. Since the uniaxial tensile test is free from friction effects, the difference between ϵ_f and ϵ_β can directly quantify the contribution of friction in formability improvement in HET. The ductility improvement is sensitive to the pre-strain at which relaxation is performed. The pre-strain in uniaxial tensile test is much less compared to HET due to necking failure in the former. Since uniaxial state of stress exist near the hole edge therefore ϵ_f corresponding to equivalent strain during HET is calculated by extrapolating eq.4 as a first approximation. ϵ_β and ϵ_f (corresponding to frictionless condition) for different combinations of interruption strain and hold time are compared in Figure 14. and tabulated in Table 7.

It is seen that in general, $\epsilon_\beta > \epsilon_f$ in all cases (Table 7) indicating definite and positive influence of friction in the formability improvement when using a servo press. Where, ϵ_f and $\Delta\epsilon = (\epsilon_\beta - \epsilon_f)$ provides the contributions of stress relaxation and friction, respectively, in time-dependent formability improvement as reported in servo press applications.

$\Delta\epsilon$ was found to be sensitive to both pre-strain and holding time, although the latter's influence was negligible as shown in Figure.15. For instance, in the case of the drilled edge, $\Delta\epsilon$ varied from 0.091 to 0.185 on increasing the pre-strain from 27.89 to 43.13; whereas, for the bored edge, $\Delta\epsilon$ varied from 0.121 to 0.334 on increasing the pre-strain from 31.84 to 44.72 This suggests that the formability improvement due to the friction effect is increased when the interruption is performed at higher pre-strain (and therefore higher stress). On increasing the hold time from 10 s to 60 s only minimal increment in $\Delta\epsilon$ is observed for both the drilled and bored edge suggesting that formability improvement due to the friction effect is mostly independent of hold time.

These observations indicate that the friction effect is primarily due to elastic recovery and pressure-dependent friction coefficient, both of which are relatively time-independent. The stress drop during interrupted HET reduces the mean stress in the contact region. Since the friction coefficient during deformation is pressure-dependent [49–51], the reduced friction coefficient contributes positively to the formability improvement. In addition to that, the elastic recovery during interruption locally changes the contact area [46], which reduces the thinning rate of the sheet and results in higher HER. However, separating the contribution of friction coefficient and elastic recovery needs additional experiments and is planned for future work.

It is of interest to note that $\Delta\epsilon$ under similar equivalent strain is different for the drilled and bored edges. The role of stress relaxation on the damage process is beyond the scope of present work, the above result provides future scope for developing time-dependent evolution of variables in a continuum damage model.

4. Conclusions

The present study reports the effect of interrupted loading on stretch-flangeability in DP600 steel. The effect is evaluated for two different edge qualities manufactured by drilling and boring. Following are the important conclusions which can be drawn from the present work.

1. Compared to monotonic HET, interrupted loading significantly increased the HER. It is shown that the effect of pre-strain plays a larger role compared to hold time during interrupted testing.
2. The influence of edge quality suggests that the damage process controlling fracture behavior is also influenced by interrupted tests.
3. The overall enhanced HER was due to the two concurrent effects, stress relaxation and friction. The contribution of stress relaxation is estimated by extrapolating an empirical equation for ductility improvement obtained from uniaxial tensile tests under similar conditions.
4. The HER improvement in the present study (including drilled and bored edges), ϵ_β, varied between 23 % to 50.3 %, of which the contribution of stress relaxation was within a narrow range of 13.9 % to 16.9 %.
5. The friction effect contributed around 9 % to 33.4 % to HER improvement. The friction effect is strongly dependent on the pre-strain and to a lesser extent on the hold time. Edge quality strongly influences the contribution from the friction effect ($\epsilon_\beta - \epsilon_I$), whereas that due to stress relaxation is relatively constant. The results indicate the transient effect on the damage evolution process controls fracture behavior in HET.

Acknowledgement

Authors would like to acknowledge ArcelorMittal for supplying the steel used in this work. Authors would also like to acknowledge DST-FIST, for funding the Scanning Electron High Resolution Microscope (FESEM) joint facility, Dept. of Mechanical Engineering and Dept. of Physics, IIT Madras. Authors would like to acknowledge Mr. Abrar Salam, Research scholar, and Mr. Sundar Kumar, Apprentice, Metal Forming Laboratory, Department of Metallurgical and Materials Engineering, IIT Madras for helping in conducting hole expansion tests. One of the authors, Kali Prasad, would like to acknowledge the help from Mr. Sahil Bharti (a Ph.D. scholar in the Mechanical Engineering Department, IIT Madras) for fruitful discussion regarding simulation work.

Appendix A. Finite element simulation

The Lankford coefficients were calculated from experiments and are tabulated in Table A.8. The HET simulations were performed assuming Hill48 anisotropic yield criterion and compared with the results predicted using von Mises yield criterion. The maximum strain in the outer edge which correlates with the onset of surface crack is predicted using both the criteria and compared in Fig.A.16. It is observed that the effect of mechanical anisotropy on the strain distribution is negligible.

Table A.8:

Coefficients of lankford parameters

r_0	r_{45}	r_{90}	$\bar{r}$
0.742	1.01	0.782	0.866

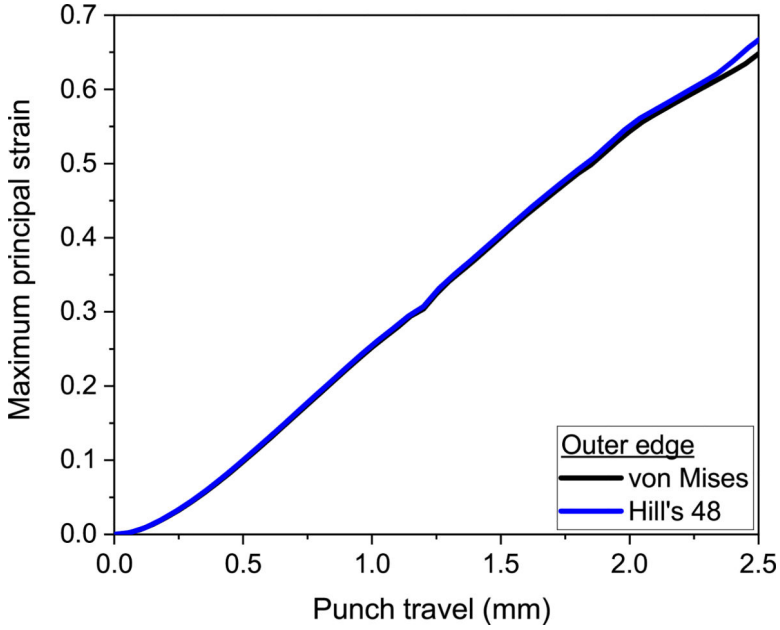

Figure A.16:
Comparison of maximum principal strain with punch travel at outer edge using Hill 48 and Von Mises criteria

Appendix B. Initial Material Characterization

The as received DP600 samples were polished for metallographic study as per standard polishing techniques and then etched with 2 % nital reagent for 10 s to obtain the as received microstructure.Scanning electron microscope (SEM) (Inspect F50 from FEI) was used to obtain the microstructure of the as received DP600 steel. For transmission electron microscopy (TEM) investigation, the as received samples were initially mechanically polished to 80 μm as per standard metallographic polishing techniques. Then 3 mm diameter discs were punched from the samples using a disc punching machine. The samples were further thinned by using a twin jet polishing machine to obtain an electron transparent region thereafter, TEM characterization was performed in FEI Tecnai G^2 operating at 200 kV. Initial surface roughness of the central hole of HET specimens prepared using drilling and boring operations was characterized using non contact optical profilometer (Wyko NT1100 Veeco Instruments, USA). Nano indentation tests using a Berkovich diamond indenter (HYSITRON Instruments) were performed to characterize the martensite and ferrite phases. The indentation tests were performed on individual phases with a maximum load of 2 mN at

the loading rate of 4 mN/min. Care was taken in selecting the appropriate indentation locations to avoid grain boundary effects.

Appendix C. Material Characterization Results

Figure.C.17(a) & (b) show the microstructure and bright field micrograph of the as received DP600 sheet obtained using a scanning electron microscope (SEM) and a transmission electron microscope (TEM), respectively. The microstructure reveals the presence of uniformly distributed martensite islands in the ferrite matrix, details of which are tabulated in Table C.9. Average grain size of the individual phases were determined using the line intercept method following ASTM E112–13 [52].

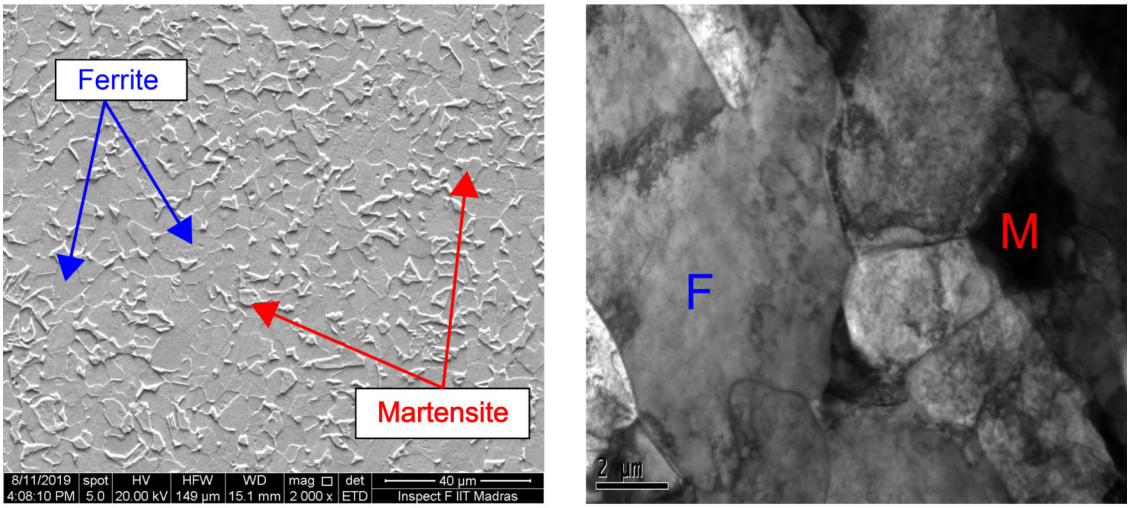

Figure C.17:
(a) Microstructure of as received DP600 steel (b) Bright field micrograph showing ferrite (F) and martensite (M) phases.

Table C.9:

Microstructural parameters of DP600 steel (uncertainties are given in ± 1 standard deviation).

Steel	Ferrite grain size (*μm*)	Martensite grain size (*μm*)	Martensite phase fraction (%)
DP600	4.1 ± 1.6	2.5 ± 1.4	22 ± 1

The hardness of ferrite and martensite phases was measured using nano-indentation tests. The indentation response of phases was estimated from the measured load vs penetration depth curves as shown in Figure.C.18. It can be seen that for a given indentation load, the average penetration depth of ferrite is higher than that of martensite, which indicates higher indentation resistance offered by martensite (Table: C.10).

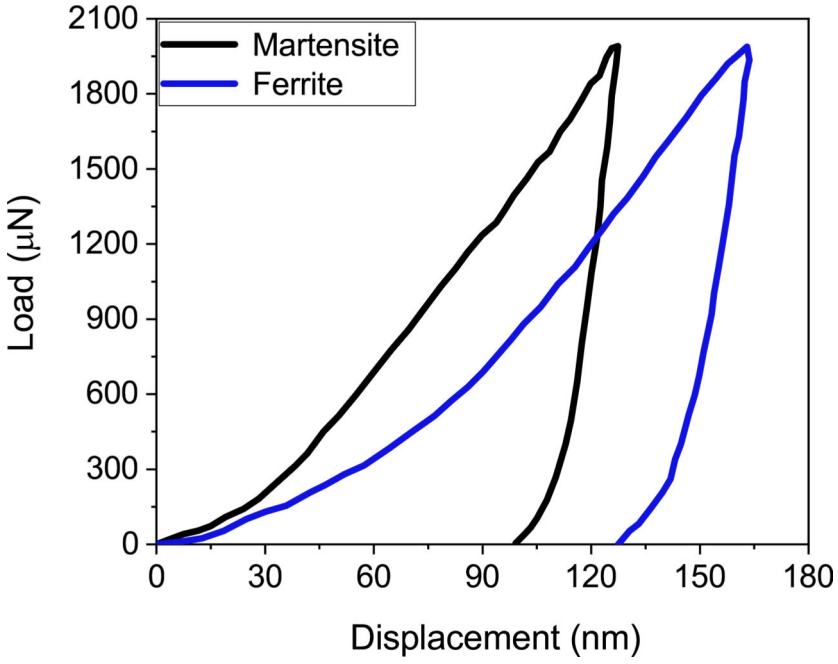

Figure C.18:
Load-displacement curves of ferrite and martensite phases for the as-received DP600 steel.

Table C.10:

Hardness characterization of DP600 steel.

Martensite phase V_m (%)	22 ± 1
Martensite Hardness H_M (GPa)	4.34 ± 0.31
Ferrite Hardness H_F (GPa)	3.49 ± 0.39

References

[1]. Qu H, Michal GM, Heuer AH, A 3rd generation advanced high-strength steel (AHSS) produced by dual stabilization heat treatment (DSHT), Metallurgical and Materials Transactions A 44 (10) (2013) 4450–4453. doi:10.1007/s11661-013-1871-z.

[2]. Walker J, Thomas DJ, Gao Y, Effects of shot peening and pre-strain on the fatigue life of dual phase martensitic and bainitic steels, Journal of Manufacturing Processes 26 (2017) 419–424. doi:10.1016/j.jmapro.2017.03.010.

[3]. Pathak C, and Butcher N, Worswick M, Assessment of the critical parameters influencing the edge stretchability of advanced high-strength steel sheet, Journal of Materials Engineering and Performance 25 (11) (2016) 4919–4932. doi:10.1007/s11665-016-2316-9.

[4]. Tasan C, Hoefnagels J, ten Horn C, Geers M, Experimental analysis of strain path dependent ductile damage mechanics and forming limits, Mechanics of Materials 41 (11) (2009) 1264–1276. doi:10.1016/j.mechmat.2009.08.003.

[5]. Chatterjee S, Bhadeshia HKDH, Stretch-flangeability of strong multiphase steels, Materials Science and Technology 23 (5) (2007) 606–609. arXiv:10.1179/174328407X179511, doi:10.1179/174328407X179511.

[6]. Cui Z, Gao L, Studies on hole-flanging process using multistage incremental forming, CIRP Journal of Manufacturing Science and Technology 2 (2) (2010) 124–128. doi:10.1016/j.cirpj.2010.02.001.

[7]. Centeno G, Silva M, Cristino V, Vallellano C, Martins P, Hole-flanging by incremental sheet forming, International Journal of Machine Tools and Manufacture 59 (2012) 46–54. doi:10.1016/j.ijmachtools.2012.03.007.

[8]. ISO, metallic materials – method of hole expanding test; 2009. http://www.iso.org [accessed may 17, 2016].

[9]. Xu L, Barlat F, Lee MG, Choi KS, Sun X, Hole expansion of dual phase steels, WIT Transactions on The Built Environment 124 (2012) 75–83. doi:10.2495/HPSM120071.

[10]. Paul SK, The effect of deformation gradient on necking and failure in hole expansion test, Manufacturing Letters 21 (2019) 50–55. doi:10.1016/j.mfglet.2019.08.004.

[11]. Taylor M, Choi K, Sun X, Matlock D, Packard C, Xu L, Barlat F, Correlations between nanoindentation hardness and macroscopic mechanical properties in DP980 steels, Materials Science and Engineering: A 597 (2014) 431–439. doi:10.1016/j.msea.2013.12.084.

[12]. Chen L, Kim J-K, Kim S-K, Kim G-S, Chin K-G, De Cooman BC, Stretch-flangeability of high Mn TWIP steel, steel research international 81 (7) (2010) 552–568. doi:10.1002/srin.201000044.

[13]. Correlation between fracture toughness and stretch-flangeability of advanced high strength steels, Materials Letters 180 (2016) 322–326. doi:10.1016/j.matlet.2016.05.145.

[14]. Comstock RJ, Scherrer DK, Adamczyk RD, Hole expansion in a variety of sheet steels, Journal of Materials Engineering and Performance 15 (6) (2006) 675–683. doi:10.1361/105994906X150830.

[15]. Casellas D, Lara A, Frometa D, Gutierrez D, Molas S, Perez L, Rehrl J, Suppan C, Fracture toughness to understand stretch-flangeability and edge cracking resistance in ahss, Metallurgical and Materials Transactions A 48 (1) (2017) 86–94. doi:10.1007/s11661-016-3815-x.

[16]. Paul SK, Correlation between hole expansion ratio (HER) and notch tensile test, Manufacturing Letters 20 (2019) 1–4. doi:10.1016/j.mfglet.2019.02.003.

[17]. Yoon JI, Jung J, Lee HH, Kim G-S, Kim HS, Factors governing hole expansion ratio of steel sheets with smooth sheared edge, Metals and Materials International 22 (6) (2016) 1009–1014. doi:10.1007/s12540-016-6346-5.

[18]. Paul SK, A critical review on hole expansion ratio, Materialia 9 (2020) 100566. doi:10.1016/j.mtla.2019.100566.

[19]. Paul SK, Effect of punch geometry on hole expansion ratio, Proceedings of the Institution of Mechanical Engineers, Part B: Journal of Engineering Manufacture 234 (3) (2019) 1–6. arXiv:10.1177/0954405419863222, doi:10.1177/0954405419863222.

[20]. Mandal GK, Ashok K, Das SK, Biswas P, Sarkar RB, Sundara Bharathy R, Srivastava VC, Development of stretch flangeable grade steels by inclusion engineering approach, Journal of Materials Engineering and Performance 27 (11) (2018) 5622–5634. doi:10.1007/s11665-018-3703-1.

[21]. Yoon JI, Lee HH, Jung J, Kim HS, Effect of grain size on stretch-flangeability of twinning-induced plasticity steels, Materials Science and Engineering: A 735 (2018) 295–301. doi:10.1016/j.msea.2018.08.052.

[22]. Calcagnotto M, Ponge D, Raabe D, Effect of grain refinement to 1m on strength and toughness of dual-phase steels, Materials Science and Engineering: A 527 (29) (2010) 7832–7840. doi:10.1016/j.msea.2010.08.062.

[23]. Fang X, Fan Z, Ralph B, Evans P, Underhill R, Effects of tempering temperature on tensile and hole expansion properties of a C-Mn steel, Journal of Materials Processing Technology 132 (1) (2003) 215–218. doi:10.1016/S0924-0136(02)00923-8.

[24]. Hasegawa K, Kawamura K, Urabe T, Hosoya Y, Effects of microstructure on stretch-flange-formability of 980 mpa grade cold-rolled ultra high strength steel sheets, ISIJ International 44 (3) (2004) 603–609. doi:10.2355/isijinternational.44.603.

[25]. Yoon JI, Jung J, Kim JG, Sohn SS, Lee S, Kim HS, Key factors of stretch-flangeability of sheet materials, Journal of Materials Science 52 (13) (2017) 7808–7823. doi:10.1007/s10853-017-1012-y.

[26]. Osakada K, Mori K, Altan T, Groche P, Mechanical servo press technology for metal forming, CIRP Annals 60 (2) (2011) 651–672. doi:10.1016/j.cirp.2011.05.007.

[27]. Maeno T, Mori K, Hori A, Application of load pulsation using servo press to plate forging of stainless steel parts, Journal of Materials Processing Technology 214 (7) (2014) 1379–1387. doi:10.1016/j.jmatprotec.2014.01.018.

[28]. Mori K, Akita K, Abe Y, Springback behaviour in bending of ultra-high-strength steel sheets using CNC servo press, International Journal of Machine Tools and Manufacture 47 (2) (2007) 321–325. doi:10.1016/j.ijmachtools.2006.03.013.

[29]. Kuo C-C, Huang H-L, Li T-C, Fang K-L, Lin B-T, Optimization of the pulsating curve for servo stamping of rectangular cup, Journal of Manufacturing Processes 56 (2020) 990–1000. doi:10.1016/j.jmapro.2020.06.004.

[30]. Stemler P, Samant A, Hofmann D, Altan T, Impact of servo press motion on hole flanging of high strength steels, in: WCX™ 17: SAE World Congress Experience, SAE International, 2017. doi:10.4271/2017-01-0311.

[31]. Yamashita H, Ueno H, Nakai H, Higaki T, Technology to enhance deep-drawability by strain dispersion using stress relaxation phenomenon, in: SAE Technical Paper, SAE International, 2015. doi:10.4271/2015-01-0531.

[32]. Hariharan K, Majidi O, Kim C, Lee M, Barlat F, Stress relaxation and its effect on tensile deformation of steels, Materials Design (1980–2015) 52 (2013) 284–288. doi:10.1016/j.matdes.2013.05.088.

[33]. Hariharan K, Dubey P, Jain J, Time dependent ductility improvement of stainless steel ss 316 using stress relaxation, Materials Science and Engineering: A 673 (2016) 250–256. doi:10.1016/j.msea.2016.07.074.

[34]. Prasad K, Krishnaswamy H, Jain J, Leveraging transient mechanical effects during stress relaxation for ductility improvement in aluminium AA 8011 alloy, Journal of Materials Processing Technology 255 (2018) 1–7. doi:10.1016/j.jmatprotec.2017.11.053.

[35]. Prasad K, Krishnaswamy H, Arunachalam N, Investigations on ductility improvement and reloading yielding during stress relaxation of dual phase Ti-6Al-4V titanium alloy, Journal of Alloys and Compounds 828 (2020) 154450. doi:10.1016/j.jallcom.2020.154450.

[36]. Astm e8 / e8m-16a, standard test methods for tension testing of metallic materials, Tech. rep, ASTM International, West Conshohocken, PA (2016). doi:10.1520/E0008E0008M – 16A.

[37]. Butcher C, Kortenaar L, Worswick M, Experimental characterization of the sheared edge formability of boron steel, IDDRG,Paris, France (2014).

[38]. Paul SK, Roy S, Sivaprasad S, Bar HN, Tarafder S, Identification of post-necking tensile stress-strain behavior of steel sheet: An experimental investigation using digital image correlation technique, Journal of Materials Engineering and Performance 27(11) (2018) 5736–5743. doi:10.1007/s11665-018-3701-3.

[39]. Varma A, Gokhale A, Jain J, Hariharan K, Cizek P, Barnett M, Investigation of stress relaxation mechanisms for ductility improvement in SS316L, Philosophical Magazine 98 (3) (2018) 165–181. doi:10.1080/14786435.2017.1398422.

[40]. Avramovic-Cingara G, Saleh Ch.A.R., Jain MK, Wilkinson D, Void nucleation and growth in dual-phase steel 600 during uniaxial tensile testing, Metallurgical and Materials Transactions A 40A (2009) 3117–3127. doi:10.1007/s11661-009-0030-z.

[41]. Saeidi N, Ashrafizadeh F, Niroumand B, Forouzan M, mofidi SM], Barlat F, Void coalescence and fracture behavior of notched and un-notched tensile tested specimens in fine grain dual phase steel, Materials Science and Engineering: A 644 (2015) 210–217. doi:10.1016/j.msea.2015.07.036.

[42]. Bandyopadhyay K, Panda S, Saha P, Baltazar-Hernandez V, Zhou Y, Microstructures and failure analyses of dp980 laser welded blanks in formability context, Materials Science and Engineering: A 652 (2016) 250–263. doi:10.1016/j.msea.2015.11.091.

[43]. Pathak N, Butcher C, Worswick M, On simulation of edge stretchability of an 800 mpa advanced high strength steel, Journal of Physics: Conference Series 734 (2016) 032121. doi:10.1088/1742-6596/734/3/032121.

[44]. Pathak N, Butcher C, Worswick MJ, Bellhouse E, Gao J, Damage evolution in complex-phase and dual-phase steels during edge stretching, Materials 4 (2017). doi:10.3390/ma10040346.

[45]. Takamura M, Murasawa K, Kusuda Y, Suzuki Y, Hakoyama T, Ikeda Y, Otake Y, Hama T, Suzuki S, Investigation on stress relaxation behavior of high-strength steel sheets based on elasto-viscoplasticity, Journal of Physics: Conference Series 1063 (2018) 012123. doi:10.1088/1742-6596/1063/1/012123.

[46]. Majidi O, Barlat F, Lee M-G, Kim D-J, Formability of ahss under an attach-detach forming mode, steel research international 86 (2) (2015) 98–109. arXiv:https://onlinelibrary.wiley.com/doi/pdf/10.1002/srin.201400001, doi:10.1002/srin.201400001.

[47]. Gil I, Mendiguren J, Galdos L, Mugarra E, de Argandona ES], Influence of the pressure dependent coefficient of friction on deep drawing springback predictions, Tribology International 103 (2016) 266–273. doi:10.1016/j.triboint.2016.07.004.

[48]. Ma X, de Rooij M, Schipper D, A load dependent friction model for fully plastic contact conditions, Wear 269 (11) (2010) 790–796. doi:10.1016/j.wear.2010.08.005.

[49]. Maeno T, Osakada K, Mori K, Reduction of friction in compression of plates by load pulsation, International Journal of Machine Tools and Manufacture 51 (7) (2011) 612–617. doi:10.1016/j.ijmachtools.2011.03.007.

[50]. yu Ben N, Zhang Q, an Meng D, gyu Lee M, Analysis of real contact area and re-lubrication in oscillating bulk forming process by corrosion method, Journal of Materials Processing Technology 253 (2018) 178–194. doi:10.1016/j.jmatprotec.2017.10.044.

[51]. yu Ben N, Zhang Q, Choi H, Bandyopadhyay K, Lee M-G, Experimental and finite element analysis on oscillating cold forming in consideration of nonlinear loading-unloading-reloading behavior, Journal of Manufacturing Processes 36 (2018) 520–534. doi:10.1016/j.jmapro.2018.10.043.

[52]. Astm e112–13, standard test methods for determining average grain size, astm international, Tech. rep, ASTM International, West Conshohocken, PA (2013). doi:10.1520/E0112-13.

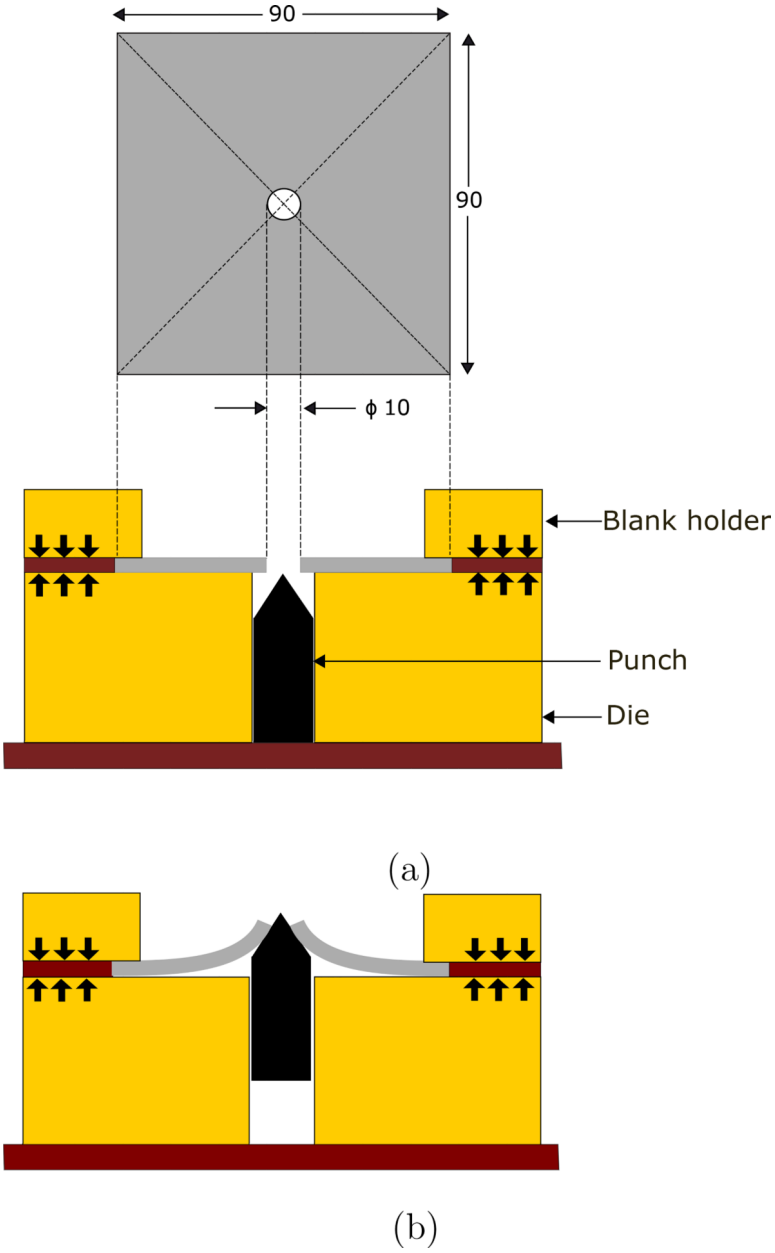

Figure 1:
A schematic diagram of the hole expansion test(a) before the test, and (b) after test completion.(All the dimensions are in mm)

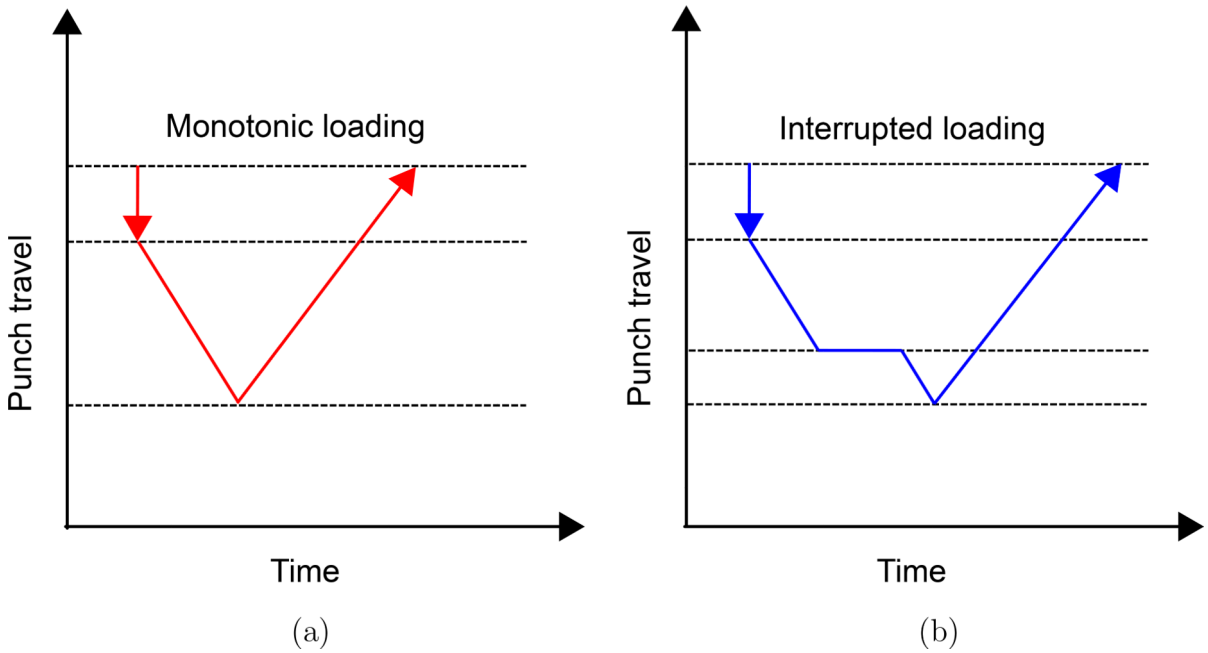

Figure 2:
Schematic diagram illustrating loading path in (a) monotonic HET and (b) interrupted HET

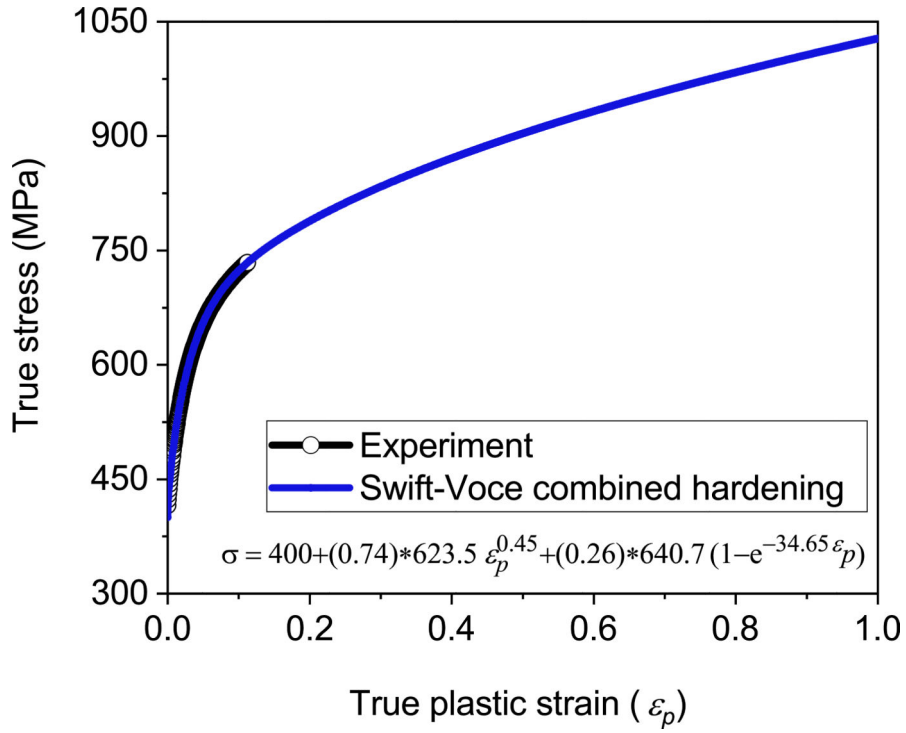

Figure 3:
True tensile stress-strain curve for a uniaxial specimen tested at a strain rate of 0.042 s^{-1} and fitted with the combined Swift-Voce hardening law for DP600 steel.

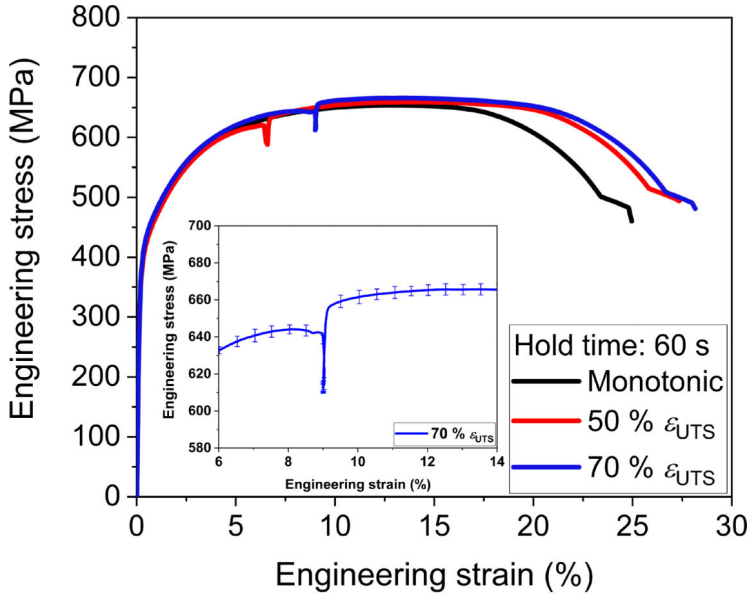

(a)

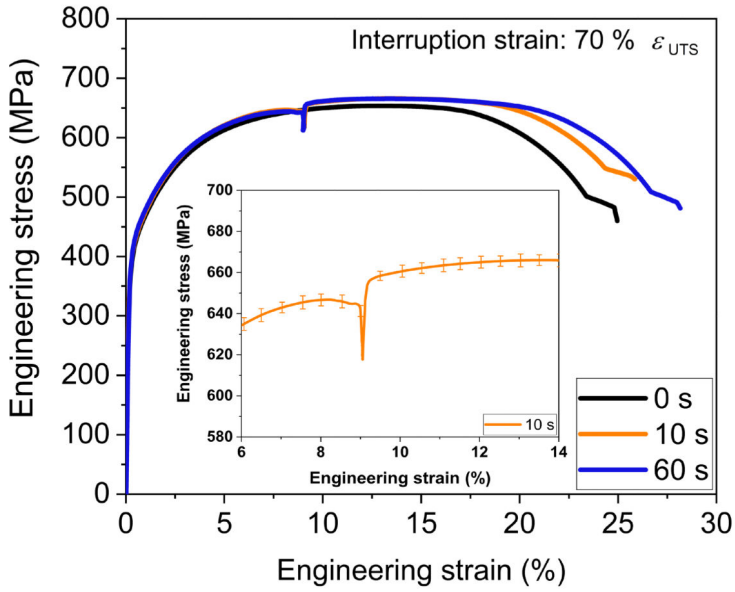

(b)

Figure 4:

Engineering stress-strain curves for uniaxial tensile specimens subjected to (a) stress relaxation for 60 s hold time at different interruption strains (b) stress relaxation at 70 % of strain corresponding to that at the UTS for different hold times tested at 0.042 s^{-1}. (Average values of stress-strain curves are reported, standard deviations for stress strain curves are shown only for few cases for clarity.)

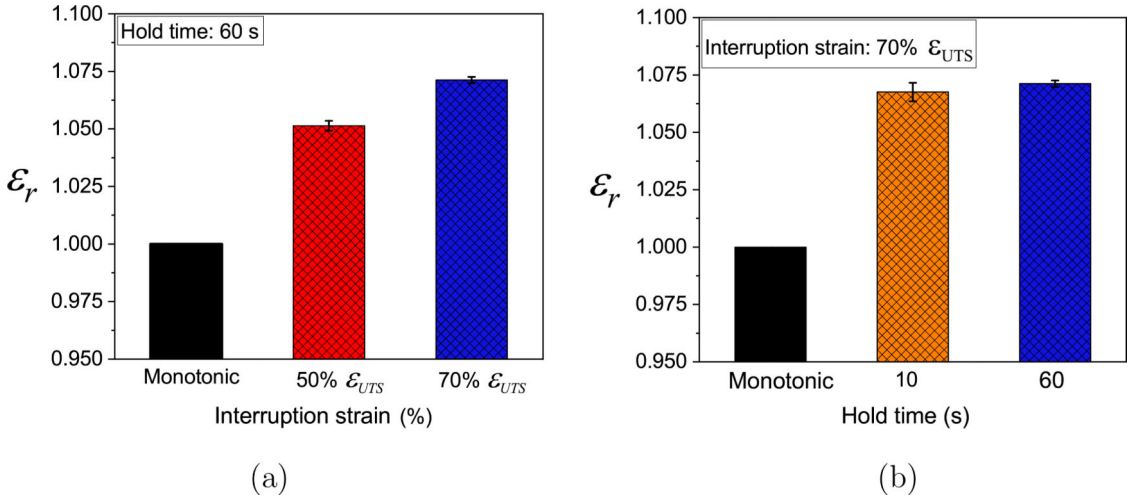

Figure 5:
Ductility improvement due to uniaxial stress relaxation test (a) effect of pre-strain (b) effect of hold time.

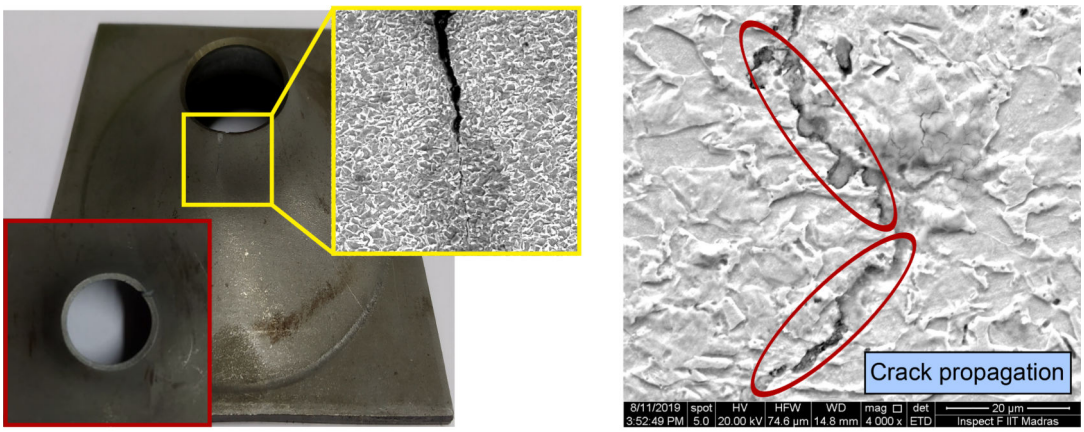

(a) (b)

Figure 6:

(a) Deformed HET sample showing the investigated region along with microstructural evidence, (b) Enlarged figure showing the crack propagation along the ferrite-martensite interface.

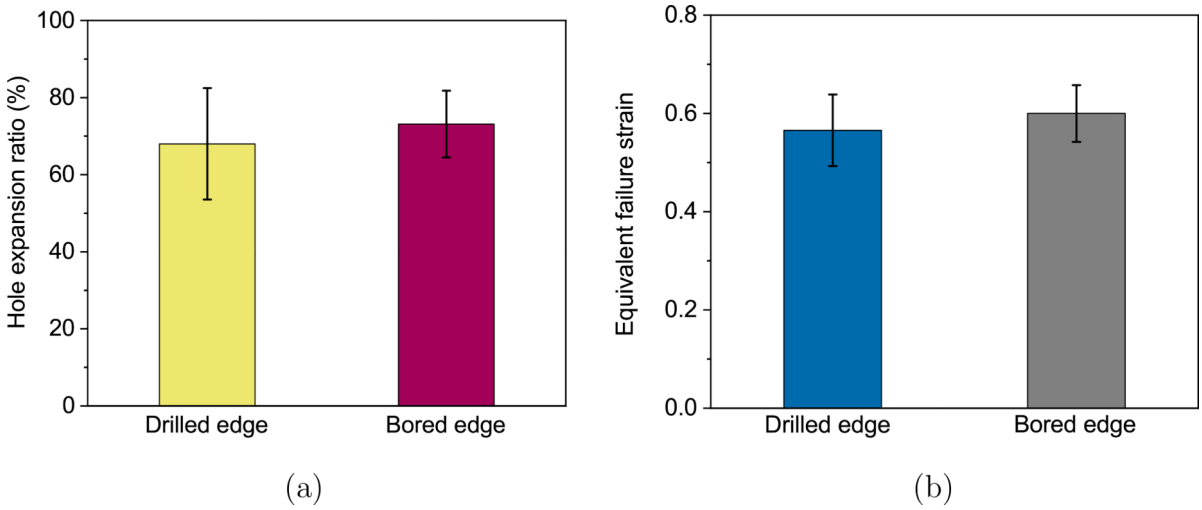

Figure 7:

Comparison of monotonic (a) Hole expansion ratios of the DP600 steel (b) Equivalent failure strain obtained during the hole expansion tests for the drilled and bored edges (Monotonic HET - samples tested without punch interruption).

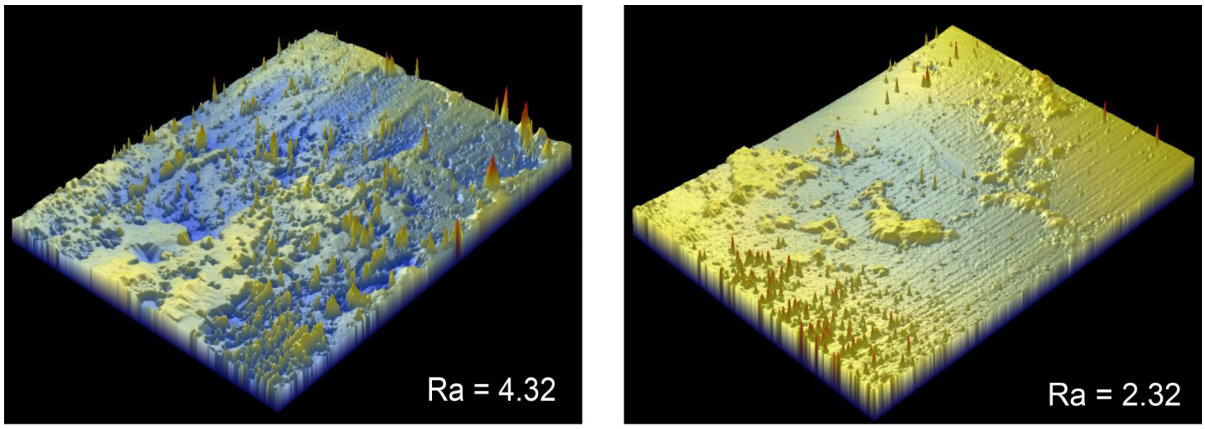

Figure 8:
Surface topography images of samples prepared using (a) Drilling (b) Boring.

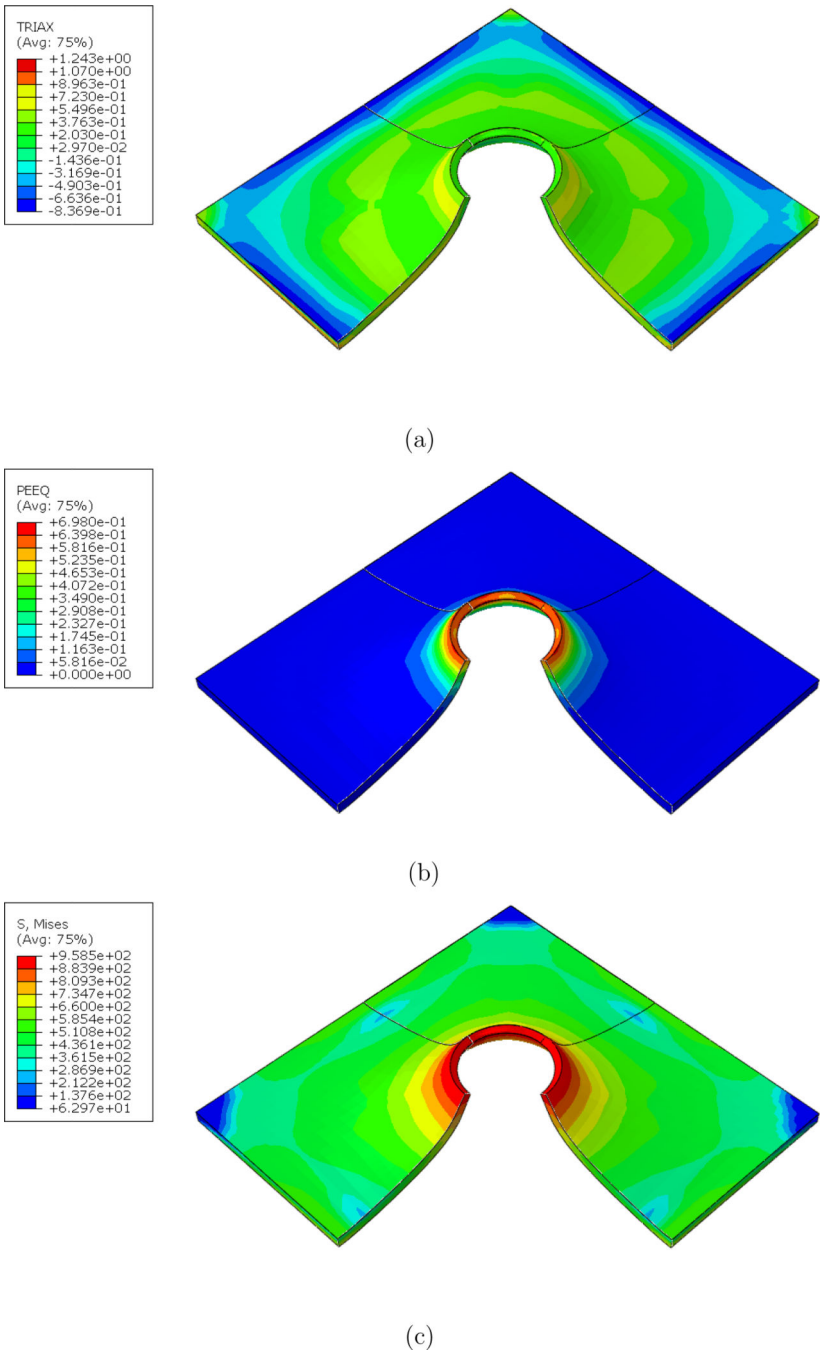

Figure 9:

Finite element simulation of hole expansion: distribution of (a) Stress triaxiality (b) Equivalent plastic strain (c) von Mises equivalent stress at the time of failure (HER = 72.36) for a drilled edge.

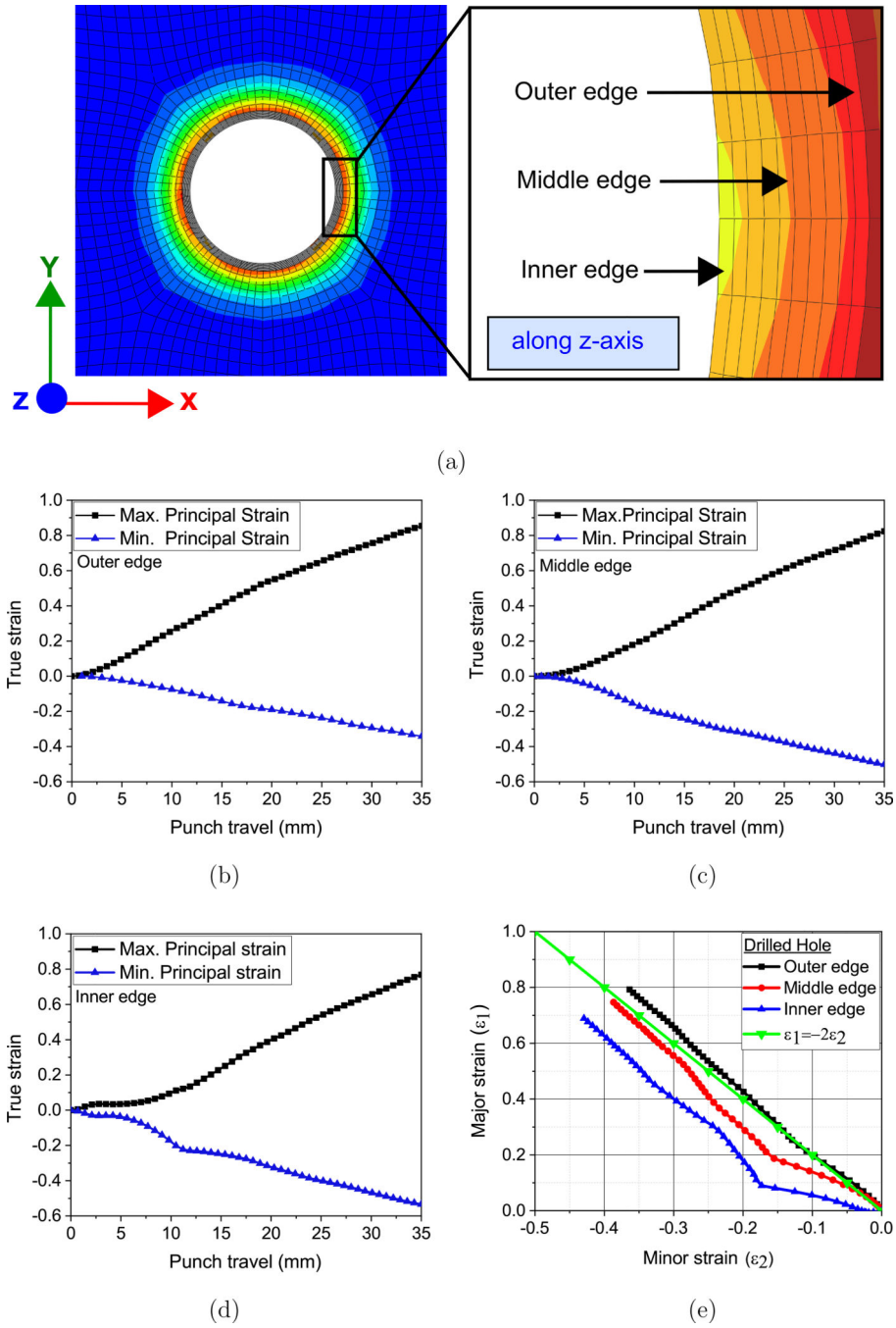

Figure 10:

(a) Deformed mesh after hole expansion test simulation. Evolution of principal strain history estimated at (b) Outer, (c) Middle and (d) Inner edge positions as a function of punch travel. (e) Strain path evolution during hole expansion test simulation suggesting uniaxial tension behavior prevails at the hole edge.

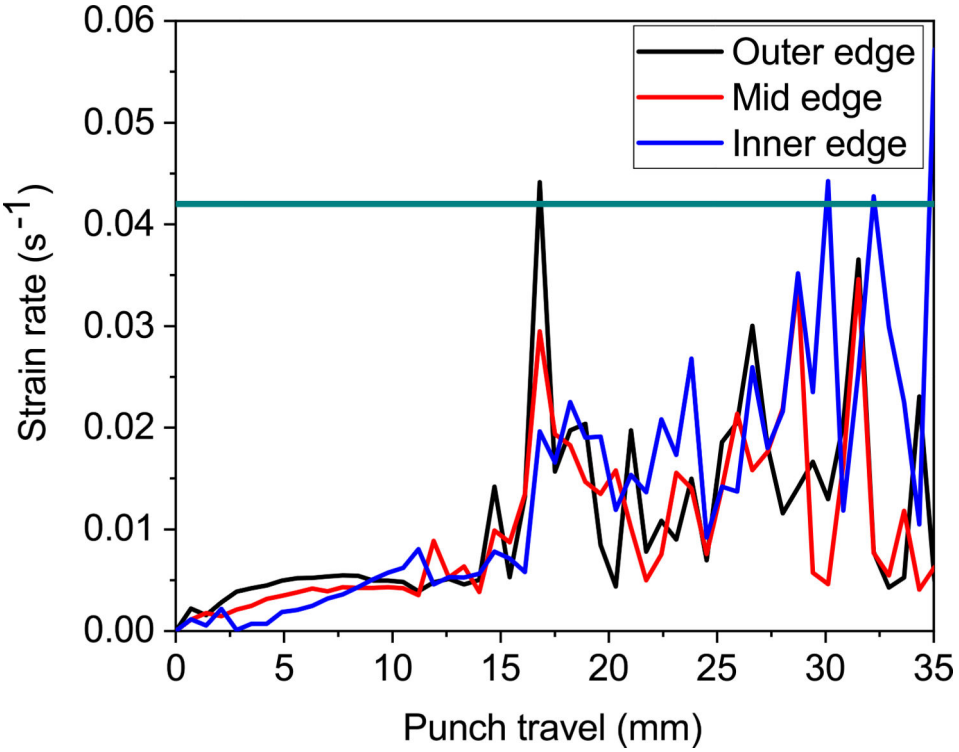

Figure 11:
Strain rate evolution estimated using finite element simulation at the hole edge when deformed using a conical punch with a constant punch velocity of 10 mm/min.

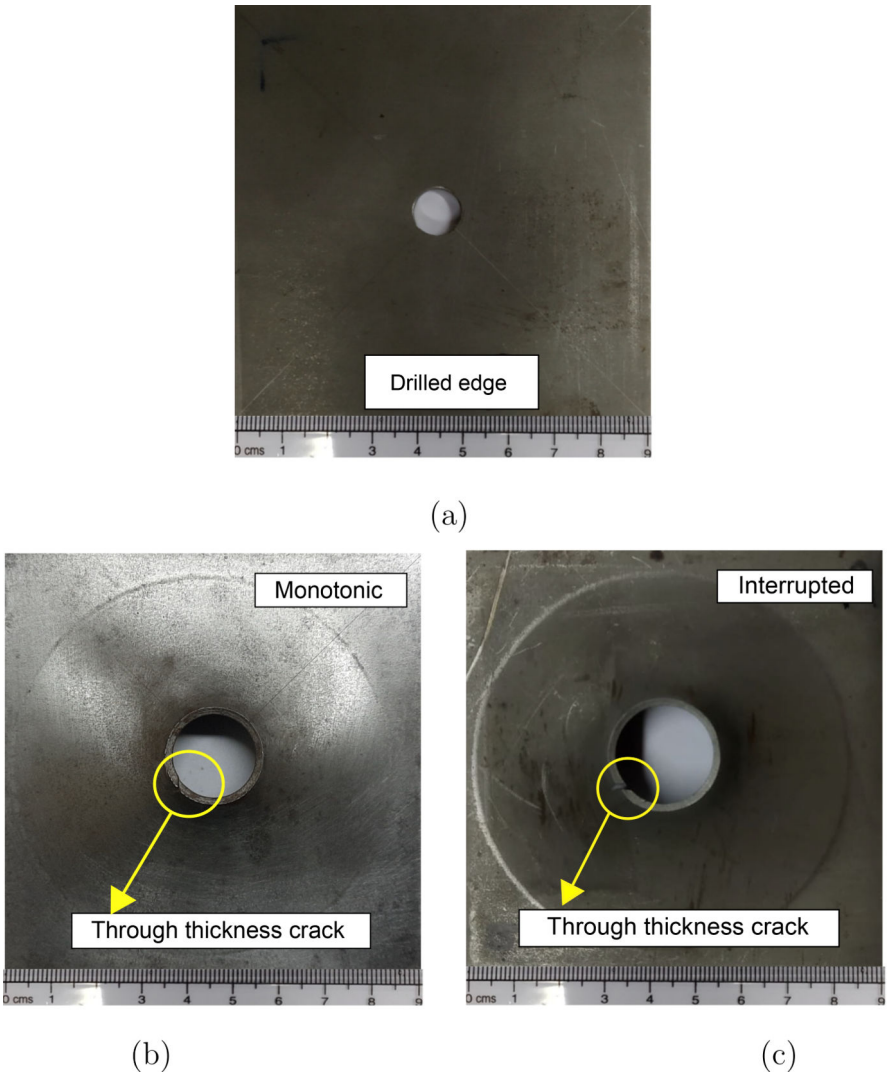

Figure 12:
(a) Initial un-deformed specimen (b) Monotonically deformed specimen, (c) Specimen deformed in interrupted loading at 50 % punch travel for 60 s.

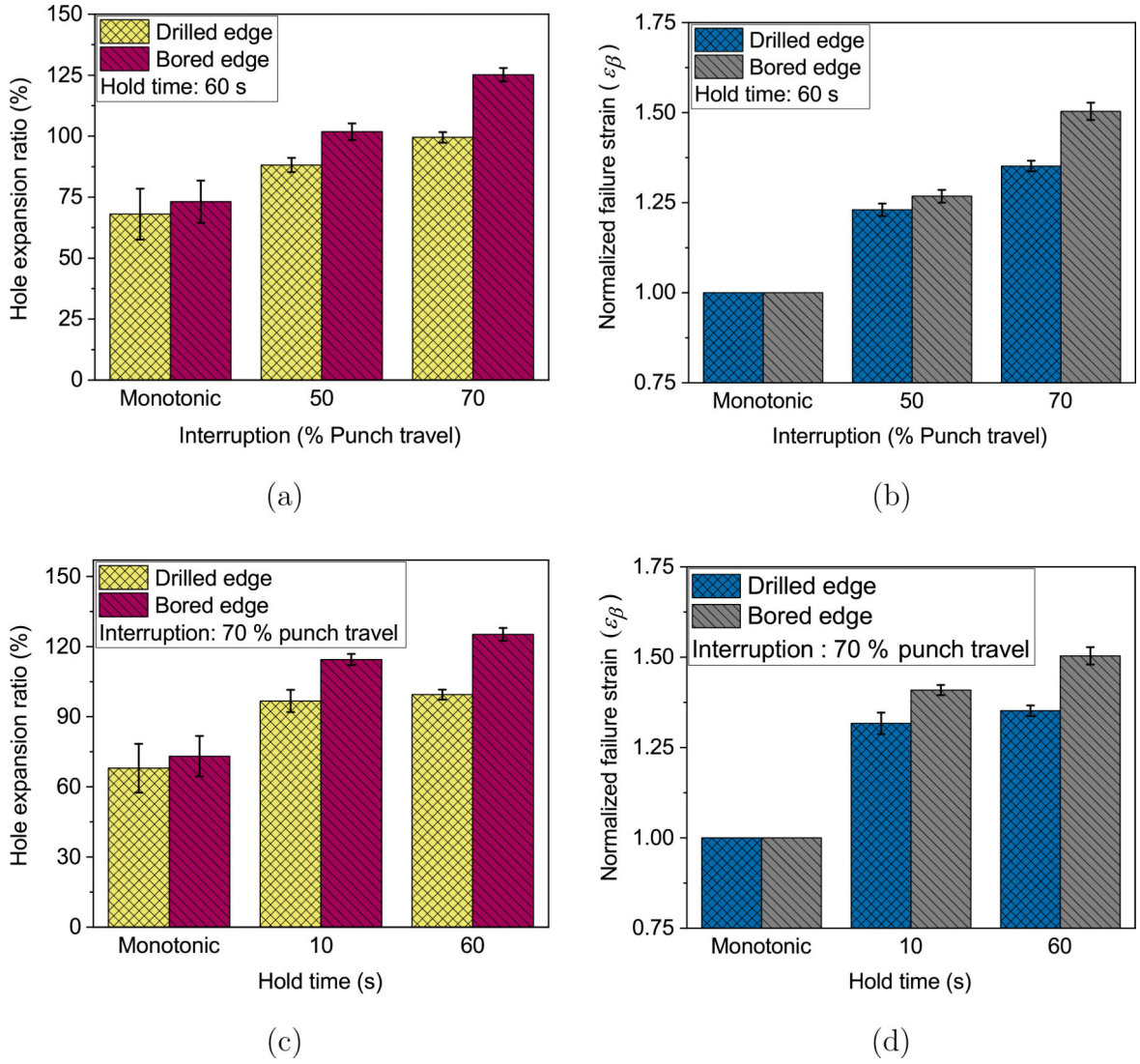

Figure 13:

(a) Improvement in HER, when tests were interrupted for 60 s at 50 % and 70 % of punch travel (b) Improvement in normalized failure strain (eq.2), when tests were interrupted for 60 s at 50 % and 70 % of punch travel (c) Improvement in HER, when tests were interrupted at 70 % of punch travel for 10 s and 60 s (d) Improvement in normalized failure strain, when test is interrupted at 70 % of punch travel for 10 s and 60 s.

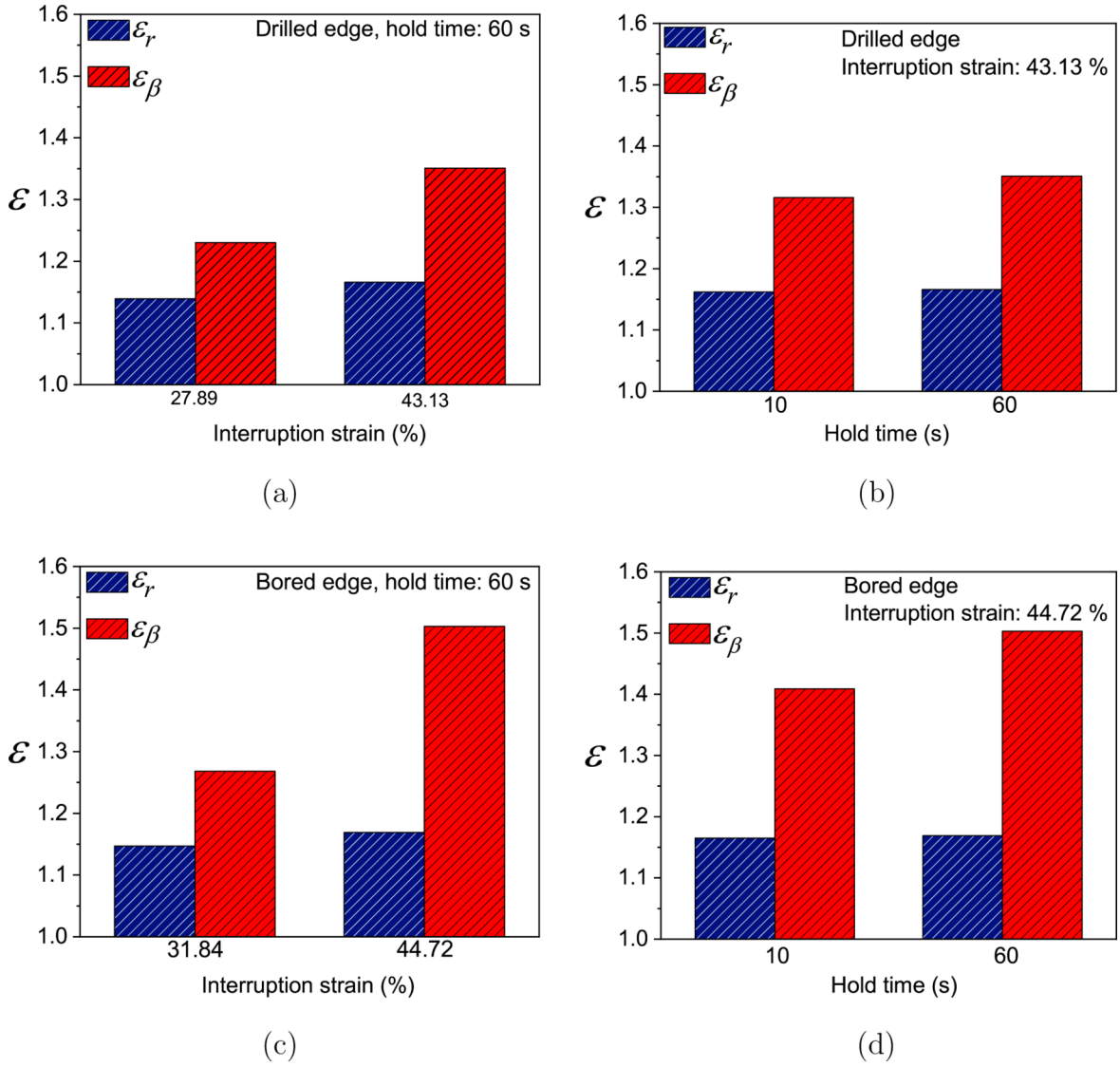

Figure 14:

Comparing uniaxial ductility improvement in frictionless conditions on deformation (ϵ_r) and HER improvement (ϵ_β) due to interrupted testing in DP600 steel (a) Effect of prestrain for drilled edge, (b) Effect of hold time for drilled edge, (c) Effect of prestrain for bored edge, (d) Effect of hold time for bored edge.

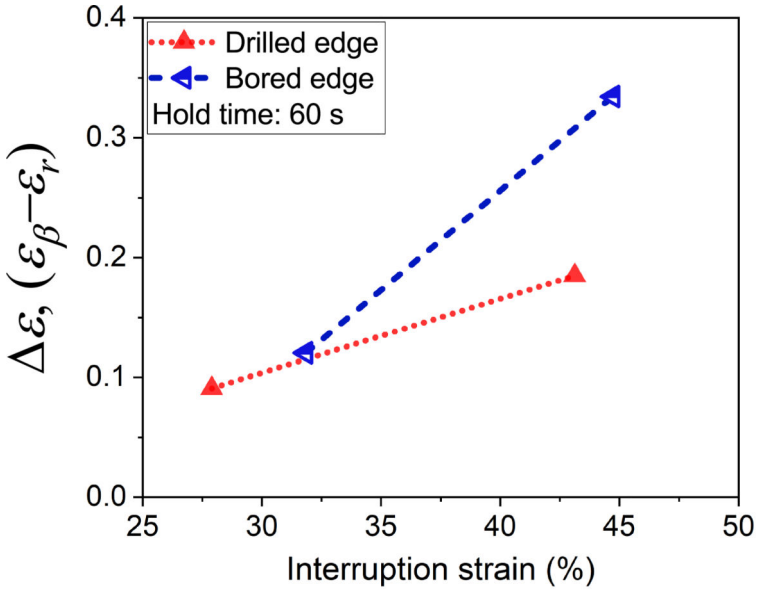

(a)

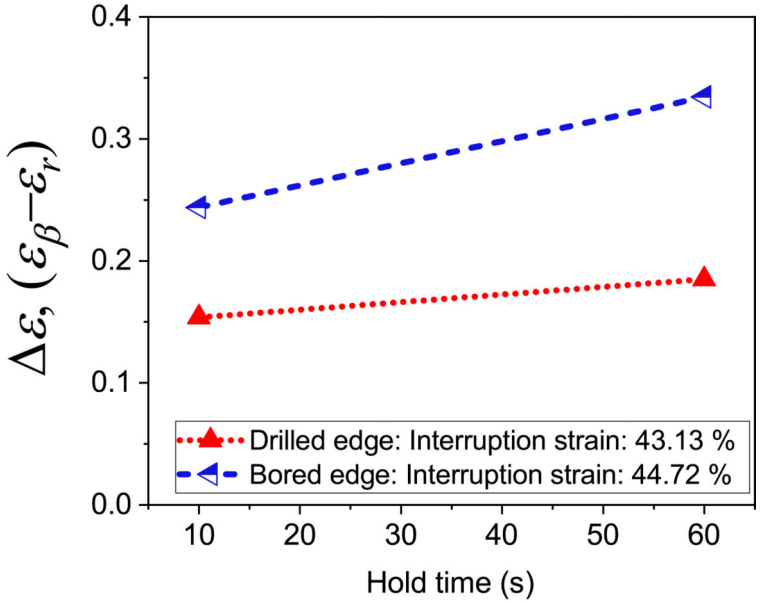

(b)

Figure 15:
Comparing the friction effect in drilled and bored edge $\Delta\epsilon = (\epsilon_\beta - \epsilon_r)$ due to interrupted HET (a) Effect of pre-strain (b) Effect of hold time.

Table 1:

Chemical composition of as-received DP600 steel (mass fraction %).

Elements	C	Si	Mn	Cr	Ni	Al	S	P	Fe
Contents(%)	0.08	0.13	0.94	0.57	0.017	0.03	0.005	0.039	Balance

Table 2:

Experimental parameters used in uniaxial stress relaxation study.

Test mode	Strain rate (s^{-1})	Interruption strain (% UTS)	Time (s)
Monotonic	0.042	-	-
Interrupted	0.042	50	60
		70	10
		70	60

Table 3:

Experimental parameters used in hole expansion tests.

Edge condition	Test mode	Interruption (% Punch travel)	Hold time(s)
Drilled edge	Monotonic	-	-
	Interrupted	50	60
	Interrupted	70	10
	Interrupted	70	60
Bored edge	Monotonic	-	-
	Interrupted	50	60
	Interrupted	70	10
	Interrupted	70	60

Table 4:

Fitting parameters of the combined Swift-Voce strain hardening law.

σ_0	z	K	n	C	a
400	0.74	623.5	0.45	640.7	34.65

Table 5:

Improvement in ductility due to uniaxial stress relaxation.

Interruption strain (% UTS)	Time (s)	Ductility improvement (%)
50	60	5.13 ± 0.002
70	10	6.75 ± 0.004
70	60	7.12 ± 0.001

Table 6:

Estimated HER and equivalent failure strain values in monotonic and interrupted test modes.

Test Mode	Interruption (% Punch travel)	Hold Time (s)	Edge Condition	HER	Equivalent failure strain
Monotonic	-	-	Drilled	68 ± 14.43	0.56±0.07
	-	-	Bored	73.12 ± 8.66	0.59±0.05
Interrupted	50	60	Drilled	88.18± 2.93	0.69±0.01
			Bored	101.83±3.40	0.76±0.01
Interrupted	70	10	Drilled	96.74 ± 4.71	0.74±0.02
			Bored	114.46 ±2.42	0.84±0.01
Interrupted	70	60	Drilled	99.48 ± 2.14	0.76±0.01
			Bored	125.17±2.74	0.90±0.02

Table 7:

Comparison of strain ratio in uniaxial tensile test and HET.

Experiment		Hold time (s)	Equivalent interruption strain (%)	ϵ_r	ϵ_β	$\epsilon = \epsilon_\beta - \epsilon_r$
Uniaxial tensile test		60	6.32	1.051	-	-
		10	8.98	1.067	-	-
		60	8.98	1.071	-	-
HET	Drilled edge	60	27.89	1.139	1.230	0.091
		10	43.13	1.162	1.316	0.154
		60	43.13	1.166	1.351	0.185
	Bored edge	60	31.84	1.147	1.268	0.121
		10	44.72	1.165	1.409	0.244
		60	44.72	1.169	1.503	0.334